Advanced High-Turning Compressor Airfoils for Low Reynolds Number Condition—Part II: Experimental and Numerical Analysis

Heinz-Adolf Schreiber

Wolfgang Steinert

German Aerospace Center (DLR),
Institute of Propulsion Technology,
D-51170 Köln, Germany

Toyotaka Sonoda

Toshiyuki Arima
Honda R&D Company,
Wako Research Center,
Saitama 351-0193, Japan

Part I of this paper describes the design and optimization of two high turning subsonic compressor cascades operating as an outlet guide vane (OGV) behind a single stage low pressure turbine at low Reynolds number condition ($Re=1.3\times10^5$). In the numerical optimization algorithm, the design point and off-design performance has been considered in an objective function to achieve a wide low loss incidence range. The objective of the present paper is to examine some of the characteristics describing the new airfoils as well as to prove the reliability of the design process and the applied flow solver. Some aerodynamic characteristics for the two new airfoils and a conventional controlled diffusion airfoil (CDA), have been extensively investigated in the cascade wind tunnel of DLR Cologne. For an inlet Mach number of 0.6 the effect of Reynolds number and incidence angle on each airfoil performance is discussed, based on experimental and numerical results. For an interpretation of the airfoil boundary layer behavior, results of some boundary layer calculations are compared to oil flow visualization pictures. The design goal of an increased low loss incidence range at low Reynolds number condition could be confirmed without having a negative effect on the high Reynolds number region.
[DOI: 10.1115/1.1737781]

Introduction

This paper contributes to modern design techniques and design considerations for improved turbomachinery blade elements. The present design is aimed at highly loaded, high turning cascades that operate as an exit guide vane in a wide Reynolds number range and especially at very low Reynolds number conditions.

Several publications on cascade investigations at low Reynolds numbers can be found in the literature ($Re<5\times10^5$, e.g., [1–3]) but little has been reported on how to design blade sections which operate at relatively low Reynolds numbers, for example in aero engine compressors at very high altitude cruise or in exit guide vanes behind turbine rotors. At Reynolds numbers below 2×10^5 profile aerodynamics become very critical and losses can increase considerably due to extended laminar and turbulent boundary layer separations. There exists a lot of experience on low Reynolds number wing section designs, e.g., [4,5], but this is of limited value for turbomachinery applications.

Therefore, a project was initiated to develop a modern numerical tool that allows automatic designs for turbomachinery blading suitable for a wide range of applications including the design of low Reynolds number airfoils. In Part I of this paper, [6], the design procedures for high turning exit guide vane cascades are described. Starting from a conventional controlled diffusion airfoil, two new highly loaded airfoils have been designed by employing two different optimization strategies. In the design process itself parametric profile generators, a Navier-Stokes flow solver, an Evolution Strategy (ES), [7], as well as a multi–objective genetic algorithm (MOGA), [8], are coupled to find cascades with superior performance, not only for the design incidence but also for off design flow angles.

Contributed by the International Gas Turbine Institute and presented at the International Gas Turbine and Aeroengine Congress and Exhibition, Atlanta, GA, June 16–19, 2003. Manuscript received by the IGTI December 2002; final revision March 2003. Paper No. 2003-GT-38477. Review Chair: H. R. Simmons.

The profiles and cascade geometry obtained after the numerical optimization process achieved considerably lower losses and a wider operating range compared to the baseline design.

Although the optimization tools do not have any understanding of the fluid-dynamical processes like the experienced aerodynamicist, they can be a valuable additional tool, since they operate unbiasedly on the design space.

The outcome of the two numerical optimizations employing ES and MOGA proved that these modern strategies can be quite successful and even applicable to very complex fluid-mechanical problems—like low Reynolds profile aerodynamics.

The aim of this second part of the paper is to validate the design process that was described in the first part, to assess the Honda Navier-Stokes blade to blade solver HSTAR, [9], that was employed, and to interpret why the optimized airfoils have a superior performance compared to the baseline airfoil. For flow analysis the HSTAR solver employes a k-ω turbulence model together with a newly implemented modified transition model according to Wilcox [10] and Drela [11].

Interpretation of the experimental results is additionally supported by comparing some typical blade Mach number distributions to the results of the viscous/inviscid blade to blade flow solver MISES of Drela and Youngren [11,12]. In particular, the blade surface boundary layer behavior of the three investigated blades is discussed with the help of simulated integral boundary layer distributions and some oil flow visualization pictures of the blade suction sides. Although all three cascades have been designed for the same flow turning, their geometry, profile Mach number distributions, and boundary layer development look quite different. Therefore, the detailed interpretation of the obtained results becomes rather difficult.

Baseline and Optimized Cascades

The cascades were designed to operate as a midsection in an outlet guide vane (OGV) behind the last turbine rotor of a small

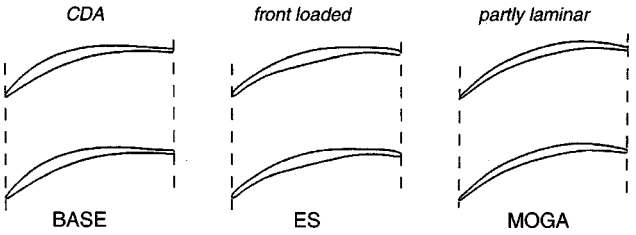

Fig. 1 Geometry of cascades

aero engine. The exit guide vane had to be designed for two-dimensional flow conditions with an inlet Mach number of 0.6 and a flow turning of about 43 deg. Especially due to the two-dimensional conditions (AVDR=1.0), the cascade is aerodynamically highly loaded and has to perform a strong diffusion down to an exit Mach number of 0.39. For the design incidence angle the diffusion factor is calculated to be approximately 0.53. Depending on flight conditions the blade chord Reynolds number varies from 1×10^6 for ground conditions to about 100,000 at high altitude cruise. In a first step a baseline cascade was designed by "hand" following the so-called controlled diffusion concept (CDA). Its suction-side Mach number distribution has a maximum at around 20% of the chord length followed by a fairly steep pressure gradient which progressively is reduced toward the trailing edge to prevent turbulent separation. This cascade, designated OGV-BASE, was designed for the high Reynolds number condition and tested in the entire relevant Reynolds number range. The calculated and measured design Mach number distribution and corresponding aerodynamic data are shown in **Fig. 1** (left). The performance was acceptable for the high Reynolds numbers but losses increased dramatically below Re=200,000 (see **Fig. 2**).

In order to improve the performance also in the low Reynolds number regime, two different optimization techniques (ES and MOGA) were applied; the principle of both methods is described in Part I. Again, the two-dimensional flow condition was assumed, the same velocity triangles as well as identical blade solidity. Because of the planned experimental validation, the freestream turbulence level during the numerical optimization was set to a value similar to the one present in the cascade windtunnel. After optimization the numerical results showed considerably lower losses in the whole Reynolds number range for both cascades although their geometry and thus the design blade Mach number distributions look quite different. **Figures 3** and **4** provide the cascade geometry and **Table 1** the design parameters.

The blade thickness in the ES optimization was prescribed; probably because of this, the OGV-ES blade looks like a "Flamingo" wing section, with maximum blade thickness concentrated at midchord location. The design blade Mach number distribution, shown in **Figs. 5** (center) and **6** (right), has its maximum at the leading edge close to $M=1.0$ followed by a steep pressure increase that successively is relaxed toward the rear. Previously Rhoden [1] found in his early low-speed experiments, that this triangular velocity distribution seems to be advantageous for the

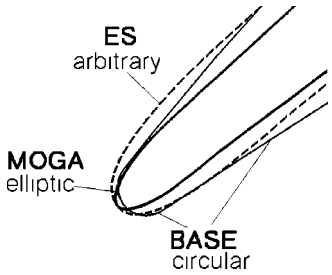

Fig. 2 Comparison of leading edge geometry

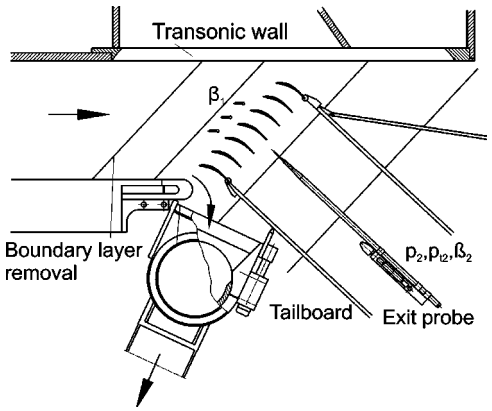

Fig. 3 Test section of DLR facility

low Reynolds number conditions, because this front loaded type of distribution tends to promote early transition without too strong laminar separations. Furthermore, the gradient of the pressure increase and the loading of the turbulent boundary layer on the rear suction side can be kept low.

The MOGA optimization produced a blade with a different blade pressure distribution, an obviously interesting alternative to the extreme front loaded design of the OGV-ES blade. MOGA came out with a slightly lower velocity peak at the leading edge, a very weak re-acceleration between 10% and 22% of chord and a moderate deceleration around midchord, forming a thin laminar separation bubble. Further along the chord an increased pressure gradient on the turbulent boundary layer is finally necessary to meet the flow turning requirement. In order to achieve low losses also at off-design incidences, the maximum blade thickness was reduced to 5.1%. The leading edge was designed elliptically to avoid the detrimental effects of the blunt circular leading edge of the OGV-BASE profile.

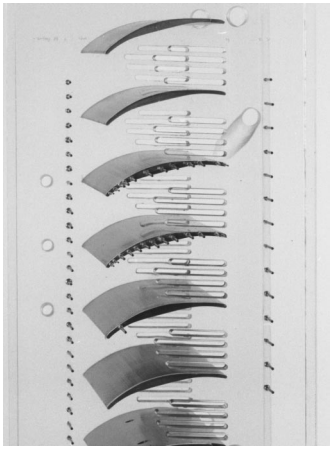

Fig. 4 Test model of OGV-ES cascade

Table 1 Cascade design parameters and results

	OGV-BASE	OGV-ES	OGV-MOGA
M_1	0.6	0.6	0.6
β_1	133 deg	133 deg	133 deg
$\Delta\beta$	43 deg	44 deg	44 deg
AVDR	1.0	1.0	1.0
D_f	0.53	0.537	0.537
LE	circular	arbitrary	elliptic
s/c	0.577	0.577	0.577
t/c	0.067	0.068	0.051

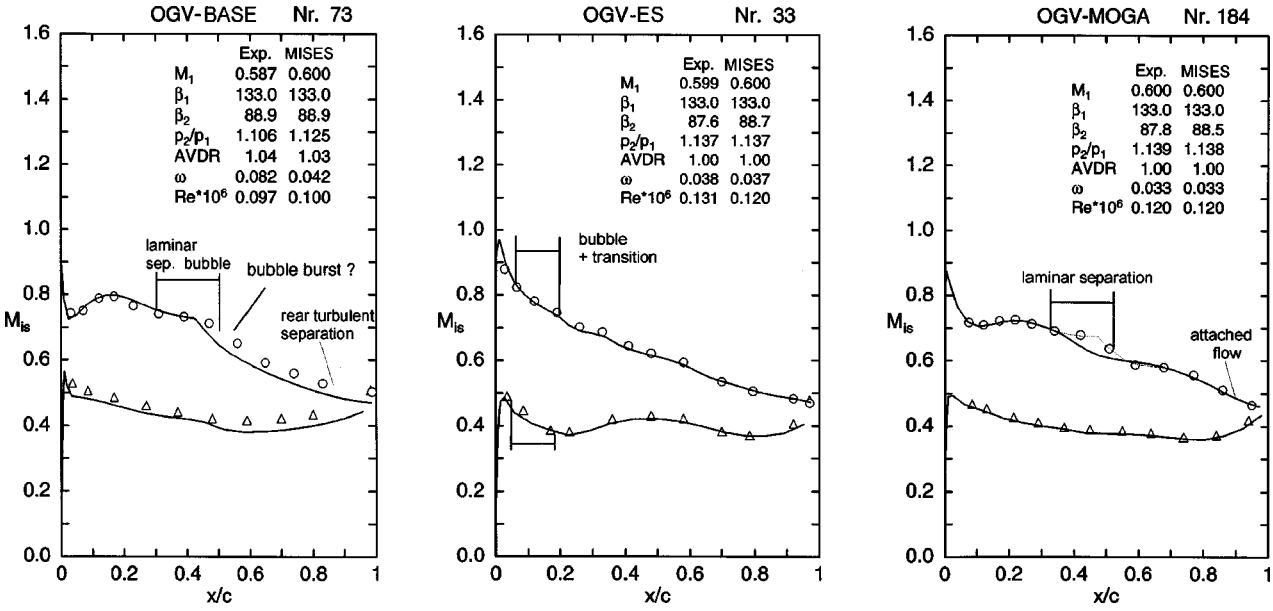

Fig. 5 Profile Mach number distributions at design incidence and Re≈120,000, experiment (symbol) and MISES simulation

Test Facility and Experimental Approach

The experiments were performed in the transonic cascade tunnel of the DLR Cologne. This tunnel is a closed loop, continuously running facility with a variable nozzle, an upper transonic wall, and a variable test section height. The air supply system enables an inlet Mach number range from 0.2 to 1.4 and a Mach number independent variation of the Reynolds number from about 1×10^5 to 3×10^6. Tunnel sidewall boundary layers ahead of the cascade are removed through protruding slots. Within the blade pack aft of the minimum pressure region endwall boundary layers were controlled by suction through chordwise slots [13] to obtain practically two-dimensional flow condition around midspan region (AVDR=1.0). Tailboards combined with throttles are used to control inlet and exit boundary conditions. For the present tests seven blades with 65 mm chord and 168 mm blade span were installed in the test section, with the center blades instrumented on the pressure and suction side. A cross-sectional view of the test section and a photograph of the cascade model are shown in **Figs. 3** and **4**.

In order to obtain tests at low Reynolds numbers, the closed loop system of the facility must be evacuated by additional sets of radial compressors. By adjusting the total pressure between 1.1 and 0.1 bar blade chord Reynolds numbers were achieved between about 900,000 and 100,000. The cascades were tested at inlet Mach numbers of 0.5, 0.6, and 0.7 in the entire possible incidence range. In this paper, results for the inlet Mach number of 0.6 are discussed. The inlet flow angle is measured with probes at the same gap-wise locations for three consecutive blade channels. Inlet total temperature is about 305 K and the freestream turbulence level around 0.6%.

Prior to the tests each individual test point has been precalculated using the blade to blade code MISES 2.4. The theoretical profile Mach number distribution, displayed real time with the test data served as a goal for the experimental distribution. By doing so, the measurement accuracy, especially for the inlet flow angle could be improved considerably.

Validation of Design and Discussion

The tests on the baseline cascade were performed in a first step and the results used to assess the blade to blade solver employed. Some results, especially the validation of the newly implemented transition model, are presented in Part I of this paper. This transition model enabled the Navier-Stokes solver to readily simulate the extension of the midchord laminar separation bubble which is particularly important for the low Reynolds number conditions.

The experimental results, especially those of the optimized blades, confirmed the design goals, in particular the design point profile Mach number distributions shown in **Figs. 5, 6**, and **7**. The off design Mach number distributions, not shown here, were met reasonably well too. Additionally, the main experimental performance data for all three cascades are summarized in **Table 2**. Here, the total pressure losses at the design incidence and the minimum losses are provided for the high and low Reynolds number conditions. For the high Reynolds numbers, losses at design incidence could be reduced from roughly 3.4% down to 2.6 or 3.2% for the ES and MOGA blade, respectively. The minimum losses are 2.2% and 2.0%, however, at negative incidences. A dramatic loss reduction was achieved for the low Reynolds number at which both new cascades showed only 3.7% and 3.3% losses compared to 8.4–10% of the OGV-BASE cascade (see **Fig. 8** (right)). In addition, the working range could be increased considerably toward the negative as well as the positive incidence.

In the following, some aerodynamic features of all three blades, the profile Mach number distributions, the incidence characteristics and the Reynolds number dependencies are discussed. In addition to the Navier-Stokes results some simulations of the profile Mach number distributions and the boundary layer parameters, using the viscous/inviscid flow solver MISES, [11,12] help to interpret the results obtained.

High Reynolds Number. The baseline cascade near its design incidence operated with a highly loaded suction side boundary layer, although it was designed following the controlled diffusion concept. Marginal increase in incidence caused rear unstable separation with a sudden loss rise; see **Fig. 8** (left) and the blade Mach number distribution of a corresponding test point in **Fig. 9** (left). Therefore, minimum losses were not obtained near design but near $\beta_1=130$ deg ($i=-3$ deg). The optimized blades overcame the problem of too strong suction side loading by reducing the gradient of the pressure increase along the whole surface. All three profile Mach number distributions are shown in **Fig. 9** and a direct comparison of the relevant suction side Mach numbers is given in **Fig. 10** (top-left). To discuss blade and boundary layer loading, plots in **Fig. 10** also provide a comparison of the simulated boundary layer displacement—and momentum thickness—

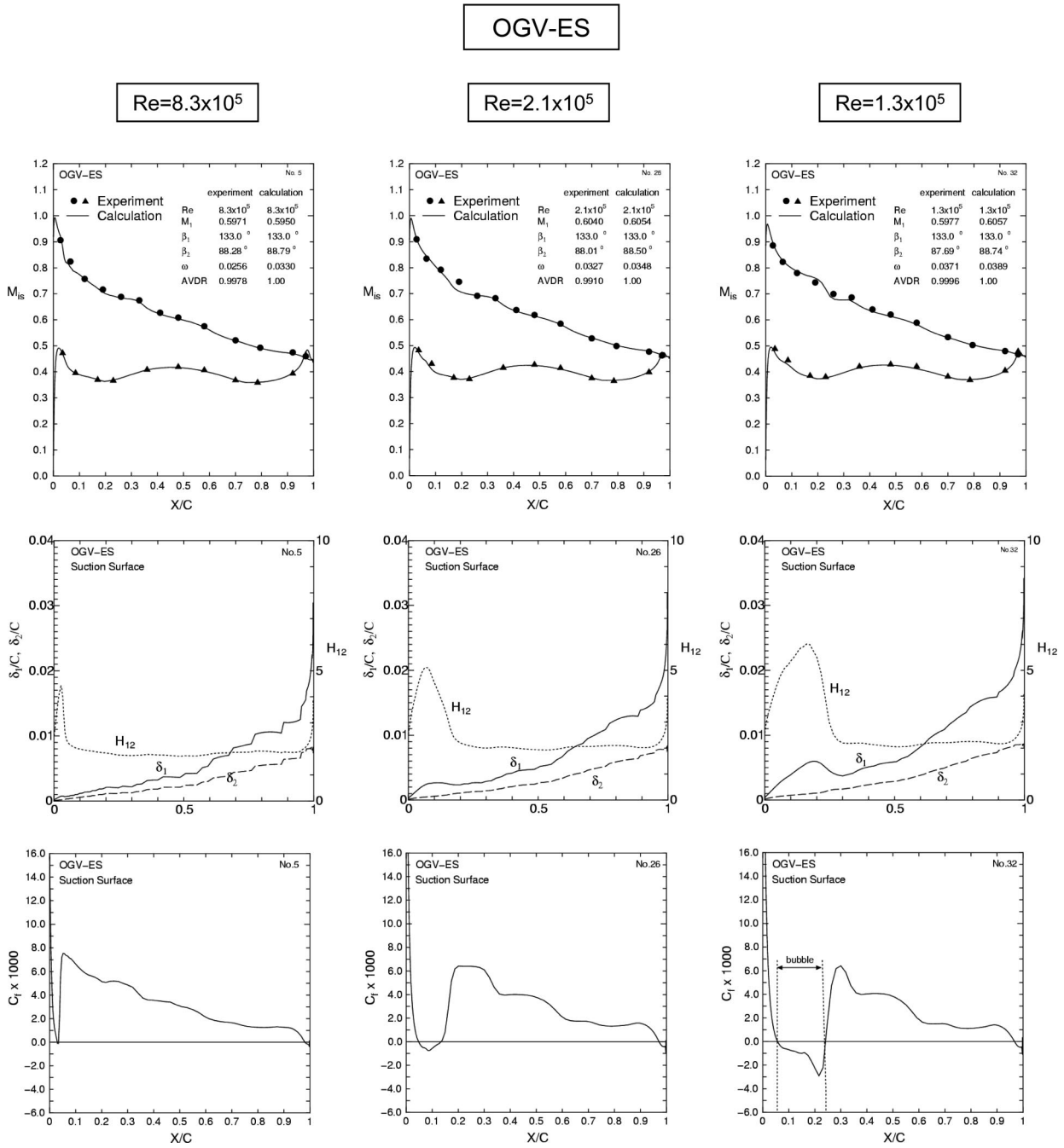

Fig. 6 Effects of Reynolds number on profile Mach number distribution and suction side boundary layer development. Experiment and HSTAR simulation, optimized cascade OGV-ES, $M_1 = 0.6$, $i = 0$ deg.

the form factor H_{12i}, and the skin friction coefficient C_f. In the plot that shows the boundary layer thickness, it is clearly visible that the ES as well as the MOGA blade both have thinner displacement and momentum thickness and therefore lower losses compared to the baseline cascade. The development of the OGV-BASE form factor H_{12i} (solid line) clearly indicates that the suction side boundary layer tends toward the separation criterion of approximately $H_{12\text{sep}} = 2.5$ relatively early, a value above which separation of a turbulent boundary layer could be expected. The ES cascade clearly stays away from separation and the MOGA blade slightly tends toward separation at the very end. Effectively, in the experiments the MOGA blade boundary layer separates from the rear suction side, clearly visible in the experimental distribution of **Fig. 9** (right), but the losses still remain relatively low.

At this high Reynolds number, boundary layer transition is observed for all three blades just after the velocity peak at the leading edge and the rest of the suction side remains turbulent. The transition process occurs within a short laminar separation bubble that forms right behind the LE and turbulent re-attachment occurs due to an intensive entrainment process along the rear part of the bubble. This local separation considerably alters the LE pressure distribution in relation to pure inviscid or turbulent flows—as it is illustrated in **Fig. 11**—and alters the state of the boundary layer from the beginning.

The LE geometry of the three blades are very different (see **Fig. 2**), the base line LE is circular and the two optimized blades have an arbitrary and elliptic geometry. Therefore, the extension of the LE bubble and the status of the boundary layer after re-attachment

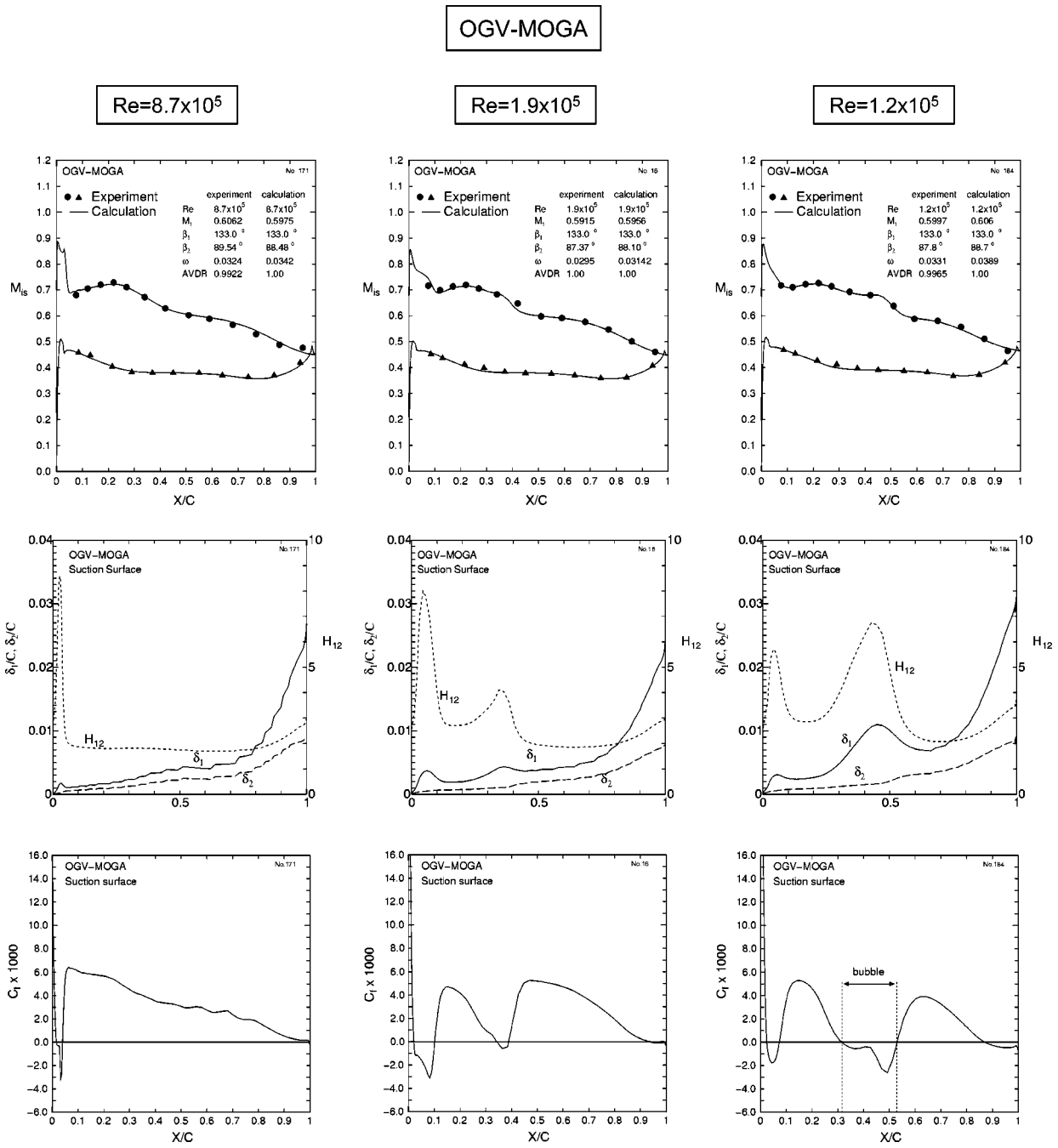

Fig. 7 Effect of Reynolds number on profile Mach number distribution and suction side boundary layer development. Experimental and HSTAR simulation, optimized cascade OGV-MOGA, $M_1=0.6$, $i=0$ deg.

Table 2 Experimental losses, flow turning and incidence range at high and low Reynolds number

	OGV-BASE	OGV-ES	OGV-MOGA
Re	0.87×10^6	0.85×10^6	0.85×10^6
ω% (i=0°)	3.4 (AVDR=1.035)	2.6	3.2
ω_{min} %	2.26 (i=−3 deg)	2.2 (i=−4 deg)	2.0 (i=−4 deg)
$\Delta\beta$ ($i=0°$)	43 deg	44 deg	44 deg
Δi ($\omega=2\omega_{min}$)	7–8 deg	13 deg	12 deg
Re	0.10×10^6	0.13×10^6	0.12×10^6
ω %	8.4–10	3.7	3.3
ω_{min} %	8.4 ($i=0$ deg)	3.7 ($i=0$ deg)	3.1 ($i=-2$ deg)

are quite different too. A zoom of the local skinfriction coefficients, shown in **Fig. 10** (bottom right), clearly indicates the different extensions of the LE bubbles. The most pronounced and concentrated velocity peak with an intensive LE separation is found on the BASE blade, even if the LE Mach number levels of the ES and MOGA blade are slightly higher. Not the absolute height of the pressure or Mach number peak is relevant, rather its local pressure gradient. Therefore, the baseline blade starts with the most critical boundary layer being disturbed from the beginning resulting in a higher risk of a rear turbulent separation with additional losses. The ES blade with the arbitrary LE geometry obviously is doing the best job; MISES (Fig. 10) as well as the HSTAR simulations in **Fig. 6** (left) both indicate no LE separa-

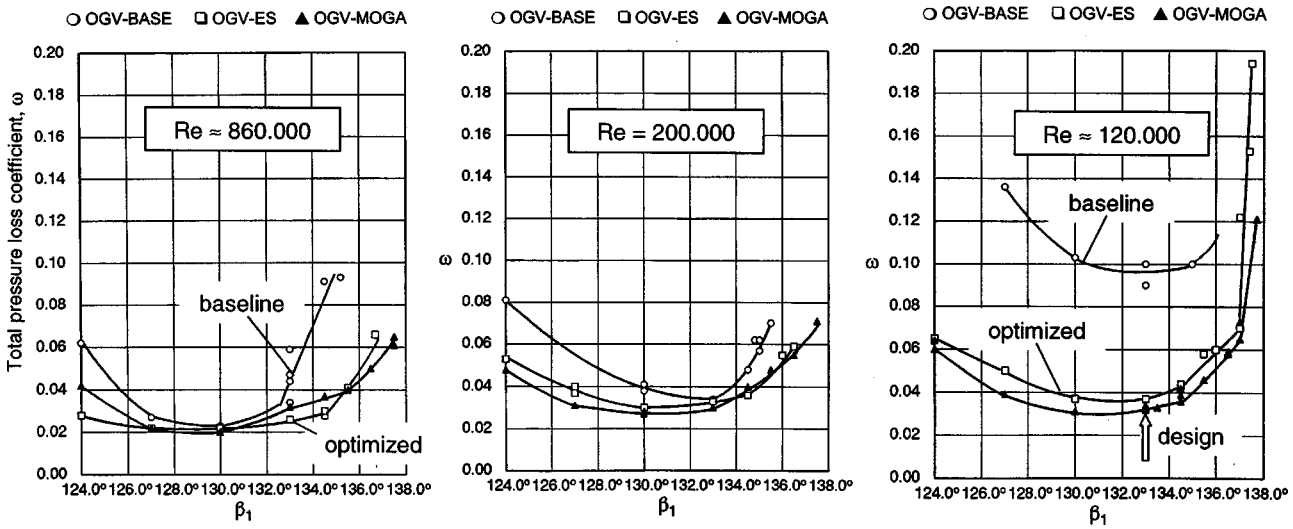

Fig. 8 Experimental loss-incidence characteristics at three different Reynolds numbers, m_1=0.6, $\beta_{1design}$=133 deg (i=0 deg)

tion, just transition, although oil flow pictures of a high Reynolds number test suggest a short bubble downstream of about 3% of chord.

In the present MISES as well as HSTAR simulations this LE peak is reasonably well simulated, but still some discrepancies between experimental losses and simulated losses are observed (see **Fig. 9**). However, Sanz and Platzer [14] found that none of their investigated transition models predicted the leading edge bubble very well, although their computational grid allowed y^+ values of the order of 1. In this context, it is suspected that with uncertainties coming from the simulation of the leading edge bubble, the boundary layer immediately behind the leading edge and further downstream may not be simulated correctly. This is more problematic especially if the rear part of the suction-side boundary layer is highly loaded and close to separation. The situation is worse if blades have circular leading edges at which the velocity peak is more pronounced with even more intensive local separations (Walraevens and Cumpsty, [15]).

The LE separation extends considerably if the Reynolds number is reduced, and it is more likely that the blade-to-blade solvers fail in simulating those local LE and severe rear separations. An example is given in test 73, **Fig. 5** (left), for which the agreement between MISES simulation and experiment is rather poor. The HSTAR simulation shows better performance both with respect to the resolution of the front peak as well as to the overall total pressure losses for the design incidence condition as shown in Fig. 14 (right) of Part I of the paper and in **Figs. 6** and **7** of the present paper. At off-design, nevertheless, some discrepancies still remain.

Low Reynolds Number. In spite of the more extended LE bubbles at the low Reynolds number, the suction side boundary layer along the front of the BASE and MOGA blade becomes laminar again and a midchord separation bubble develops. At this low Reynolds number. the BASE blade boundary layer fully separates from the suction side and losses increase to about 8–10%

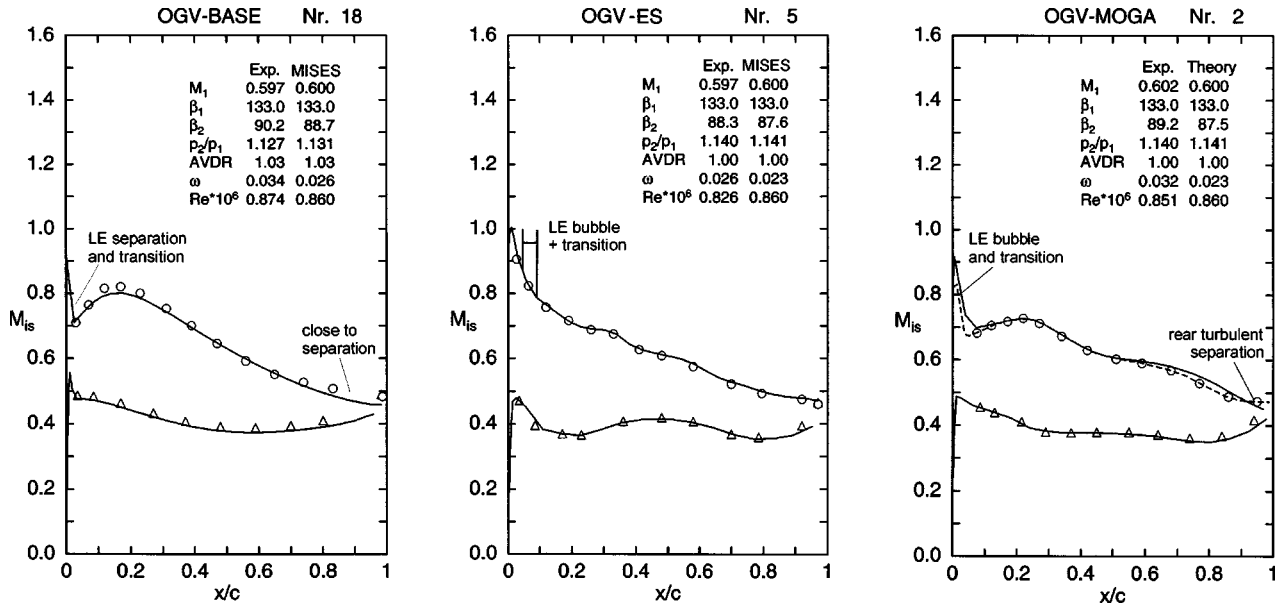

Fig. 9 Profile Mach number distributions at design incidence and Re=860,000, experiment (symbol), and MISES simulation

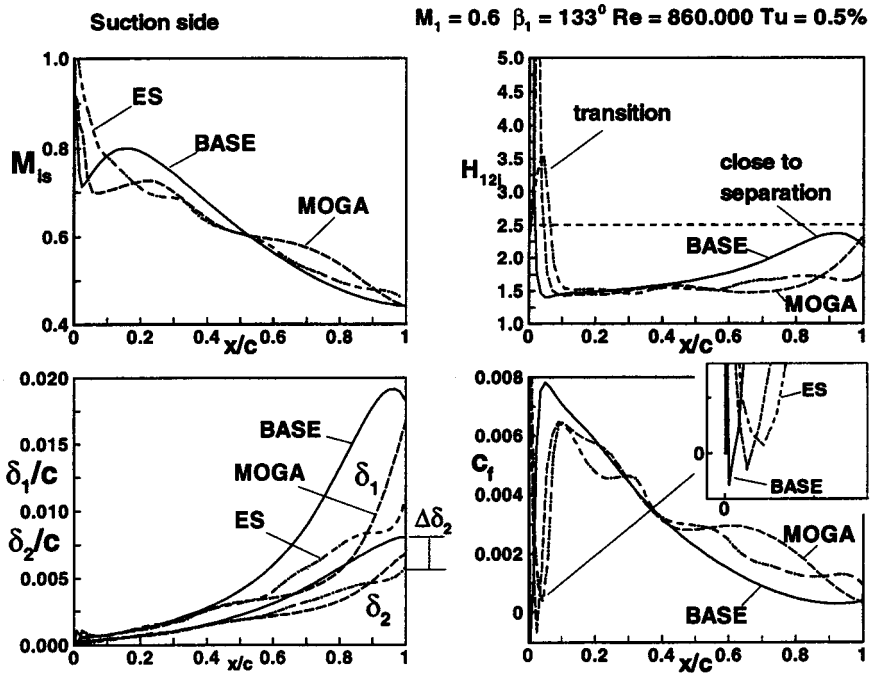

Fig. 10 Discussion of suction side boundary layer parameters at Re=860,000 (MISES simulation)

(**Fig. 5** (left)). In contrast, both optimized blades show losses of only 3.3 to 3.7% at Reynolds numbers around 120,000.

Due to the reduced adverse pressure gradient on the MOGA blade its midchord bubble is less pronounced and produces lower losses. Furthermore, the flow entrainment process during reattachment at the rear part of this bubble introduces new turbulent energy into the rear suction side boundary layer so that trailing edge separation is suppressed, which is visible in **Fig. 5** (right). From **Fig. 5** we realize that MISES, which was run with a free stream turbulence level of 0.5%, slightly underpredicts the extension of the midchord bubbles whereas HSTAR with the newly implemented transition model meets the bubble extensions reasonably well, as can be seen in **Figs. 6** and **7** as well as in Fig. 15 of Part I of the paper.

The front loaded ES blade design shows a more extended but thin bubble downstream at approximately 6% of chord with transition completed near 22%. The experimental and the simulated form factors, both do not indicate any rear turbulent separation, see **Figs. 5** (center) and **6**.

Incidence Characteristics. **Figure 8** provides the experimental total pressure losses for the entire investigated incidence range for Reynolds numbers around 8.6, 2.0, and $1-1.2\times10^5$. All three figures clearly show the essential advantage of the optimized blades: lower design point losses as well as a more wide incidence range. It is clearly visible in **Figs. 8** and **12** that the location of minimum losses is shifted from negative incidences ($i=-3-4$ deg) toward the design incidence ($\beta_1=133$ deg) if the Reynolds number is reduced (see also **Table 2**). At Re=200,000 the baseline cascade still has reasonably low losses, but for Re $\leqslant$130,000 the blade separates and losses increase considerably.

Both optimized blades achieved their design goal and losses remain low in the entire Reynolds number range. It is difficult to decide, which of the two cascades is superior: At the high Reynolds number and at the design incidence ($\beta_1=133$ deg) the MOGA blade separates slightly, but it seems to be marginally better over the entire incidence range at low Reynolds numbers.

Navier-Stokes Analysis. The experimentally observed loss-incidence characteristics are reproduced by the HSTAR solver reasonably well at least for the low Reynolds number conditions, as can be seen in **Fig. 13**. Also the high Reynolds number tests (**Fig. 14**) at $i=0$ deg were met, but the losses in the negative and positive incidence range differ considerably. This is true especially for the baseline cascade that showed an unstable suction side separation beyond $\beta_1=133$ deg in the experiments. However, the numerically simulated losses seem to be too high, not because of boundary layer separation, but rather due to high ''numerical losses'' within the entire flow field. There are probably

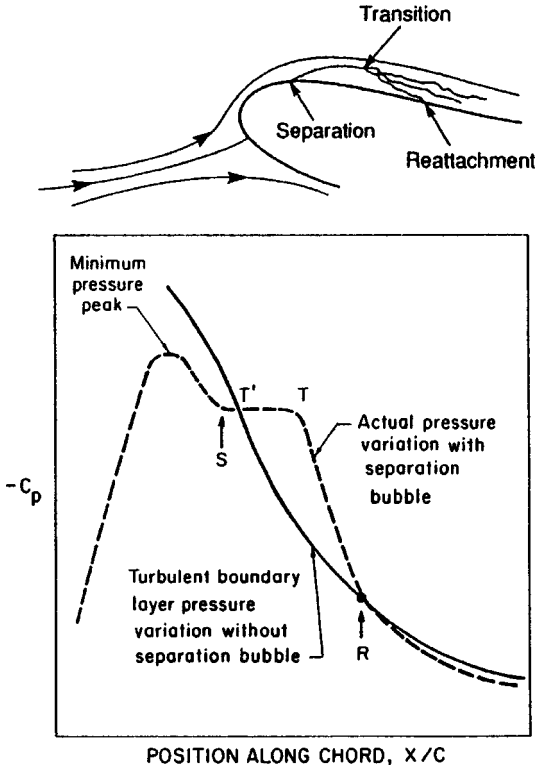

Fig. 11 Principle of LE separation (Mueller [5])

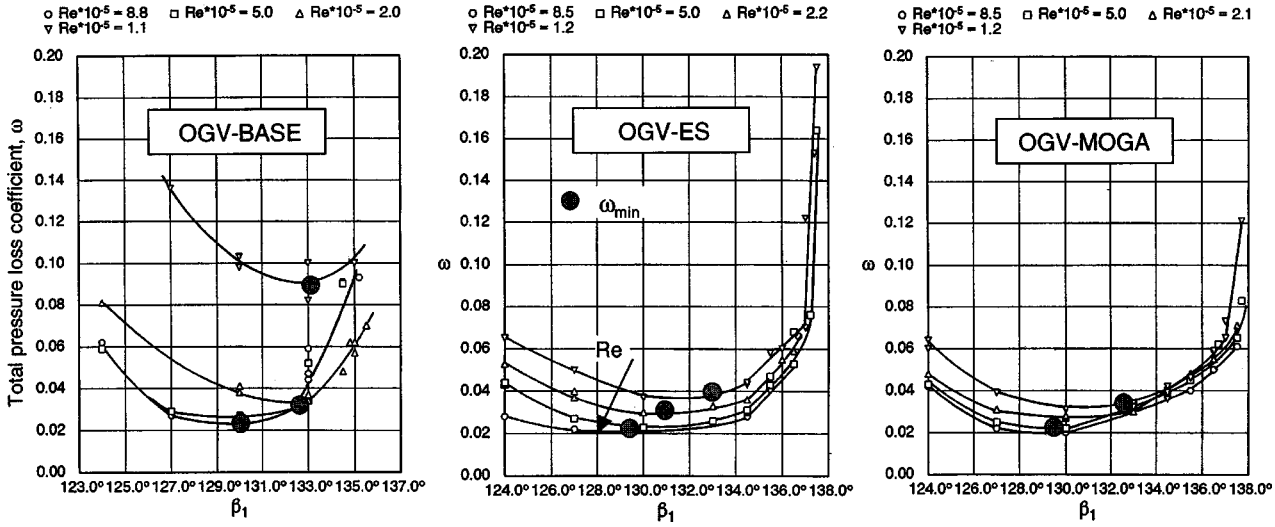

Fig. 12 Influence of the Reynolds number on the loss-incidence characteristics, $M_1=0.6$

several reasons for the discrepancy between the experimental losses and the numerical ones, and it is beyond the scope of this paper to investigate all of these. However, according to the assessment of different turbulence models (Chien's low Re k-ε and low Re k-ω) with the same numerical platform (computational grid and flow solver), there seems to be a general tendency that the losses from the k-ω turbulence model without the viscous modifications near the wall are high for the attached flow (not shown here). This may be caused by the overestimation of the turbulent energy due to the absence of a damping function in the k-ω model and/or due to the overproduction of turbulence, as pointed out by Michelassi et al. [16] for their calculations near the leading edge of turbine blades. Regardless of this disadvantage, the reason why we adopted the k-ω model without the viscous modifications, [10], for all calculations in this work is because this model is suitable for the introduction of the intermittency-based transition model and shows relatively better results than the others for the entire low Reynolds number condition.

Reynolds Number Characteristics. From **Fig. 12** that shows the experimental loss incidence characteristics of all three cascades, plots were derived to display the loss ~ Reynolds number dependency at three characteristic incidences. For all incidence angles it is clearly visible that the optimized blades ES and MOGA are superior to the baseline cascade in the entire Reynolds number range, whereby most improvements were achieved for Reynolds numbers below 200,000. As can be seen from **Fig. 12**, minimum losses are measured around $i=-3-4$ deg for all cascades in the high Reynolds number regime. The corresponding plot of the Reynolds number characteristics at this minimum loss incidence ($i=-3$ deg in **Fig. 15** (left)) clearly reveals the classical tendency with a marginal loss rise between 9 to 5×10^5, but an intensive loss increase below a certain "critical" Reynolds number, pronounced especially for the baseline cascade. For all three incidence angles shown in **Fig. 15**, a distinct "critical" Reynolds number for the optimized blades could not be recognized, at least not until the Reynolds numbers approach values of $1.0-1.2\times10^5$.

It is worth mentioning that the MOGA blade losses seem to be more or less independent of the Reynolds number, a slightly strange behavior. But this can be explained by the observation that the MOGA blade starts to separate at the high Reynolds number condition and not at the low Reynolds numbers, as was explained

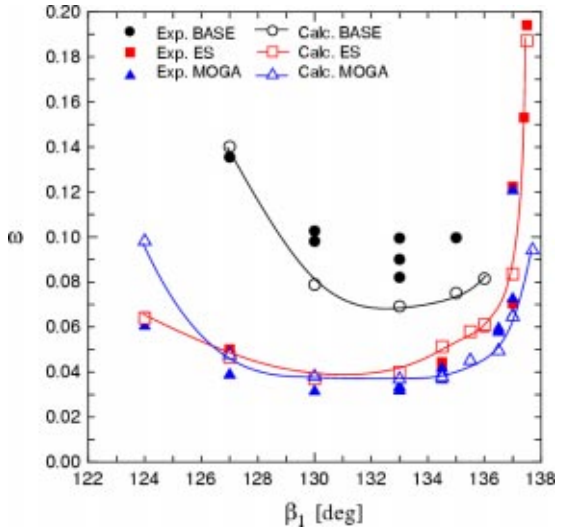

Fig. 13 Incidence characteristic at the low Reynolds number, HSTAR simulation and experiment, Re≈1.0–1.2×10^5

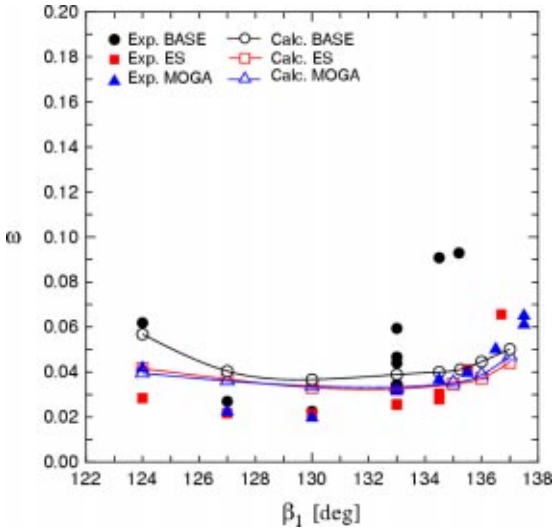

Fig. 14 Incidence characteristic at high Reynolds number, HSTAR simulation and experiment, Re≈8.6×10^5

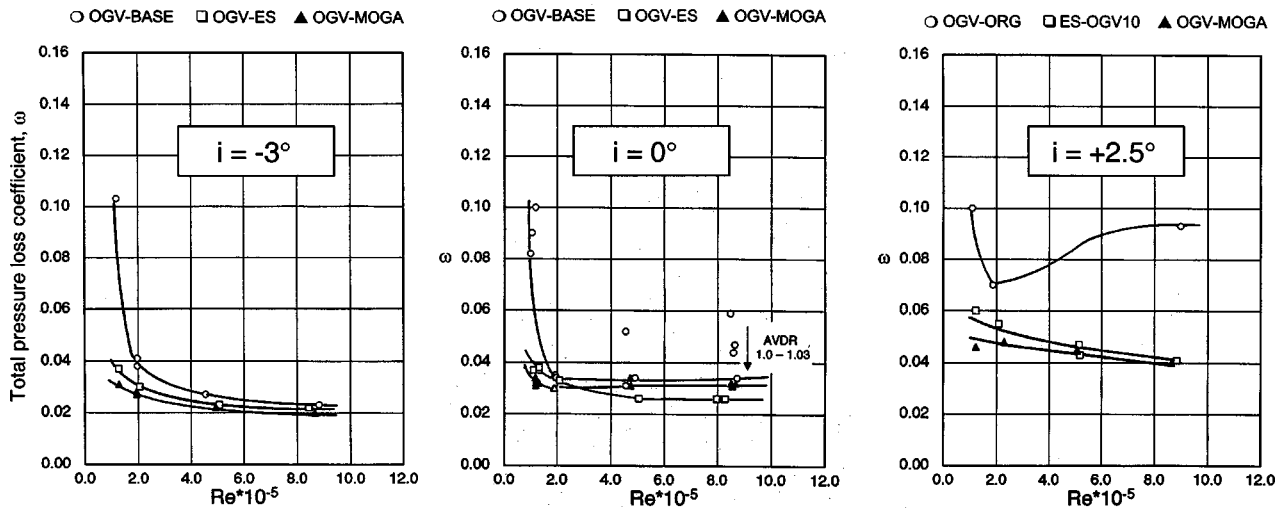

Fig. 15 Effect of the Reynolds number on experimental losses at three incidence angles, $M_1 = 0.6$

already in the previous section. A similar effect, i.e., that losses are relatively reduced when the Reynolds number decreases, can be observed with the baseline cascade for $i = 0$ and $+2.5$ deg. Around the Reynolds number of 200,000, there seems to be a loss minimum. It is presumed that for these conditions the turbulent flow entrainment process at the rear part of the laminar separation bubble has a positive effect on the turbulent boundary layer; as a result the rear (turbulent) boundary layer separation is suppressed or reduced.

Oil Flow Visualization

Oil flow visualization tests have been performed for conditions at high and low Reynolds numbers to study the blade surface boundary layer development. Our focus is the blade suction side at the low Reynolds number condition, the results of which are discussed below. The interpretation of the oil flow pictures is supported by the results of corresponding boundary layer calculations from the viscous/inviscid solver MISES. The calculations were performed at the experimental Reynolds number, but the freestream turbulence level was adjusted in such a way that the extension of the simulated laminar separation bubble is approximately in accordance with the extension observed in the experiment.

Particularly delicate was the interpretation of the tests for the baseline cascade (BASE) because it showed an unstable midchord laminar separation bubble. **Figure 16** provides results for the BASE cascade at design incidence and at a Reynolds number of 190,000, conditions under which the losses of this blade are still on a relatively low level of 3.7–4%. The oil streak lines indicate laminar flow until 29–30% and an unstable midchord separation bubble or rather a bubble that disappeared intermittently with an onset of intermittent rear turbulent separation. It is assumed that in the experiment, the local separation bubble behind the circular LE partly induces a destabilization of the shear layer and triggers the suction-side boundary layer to become turbulent. In this situation, the bubble disappeared but the rear suction side boundary layer separated. With the help of MISES these two observed situations, a laminar midchord bubble and a rear turbulent separation, could be simulated either by assuming a very low turbulence level of 0.05%, by which the experimental bubble length was met, or with a turbulence level of 0.5%, to obtain rear turbulent separation. The

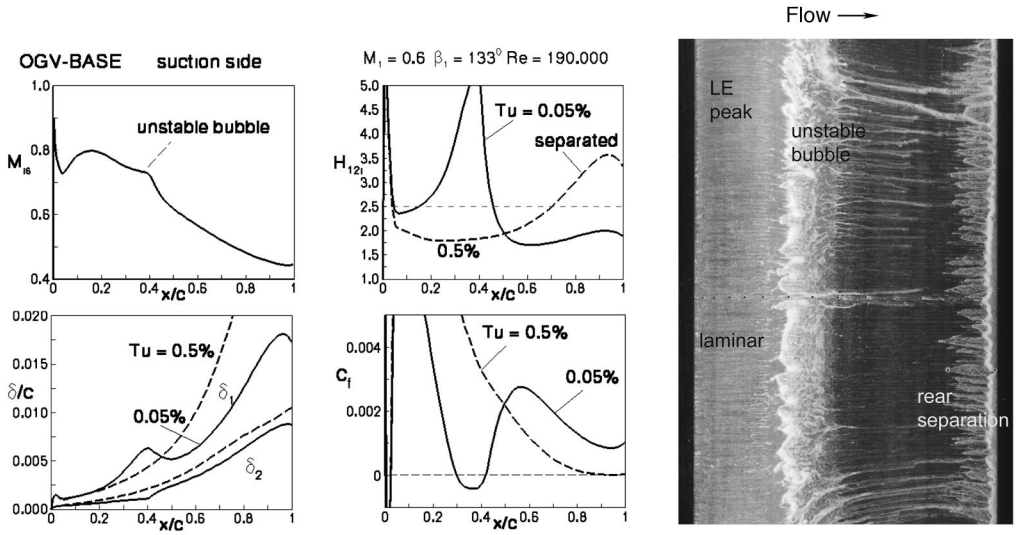

Fig. 16 MISES suction side boundary layer parameters of OGV-BASE for $Tu = 0.05$ and 0.5% and oil flow picture at $i = 0$ deg and Re≈190,000

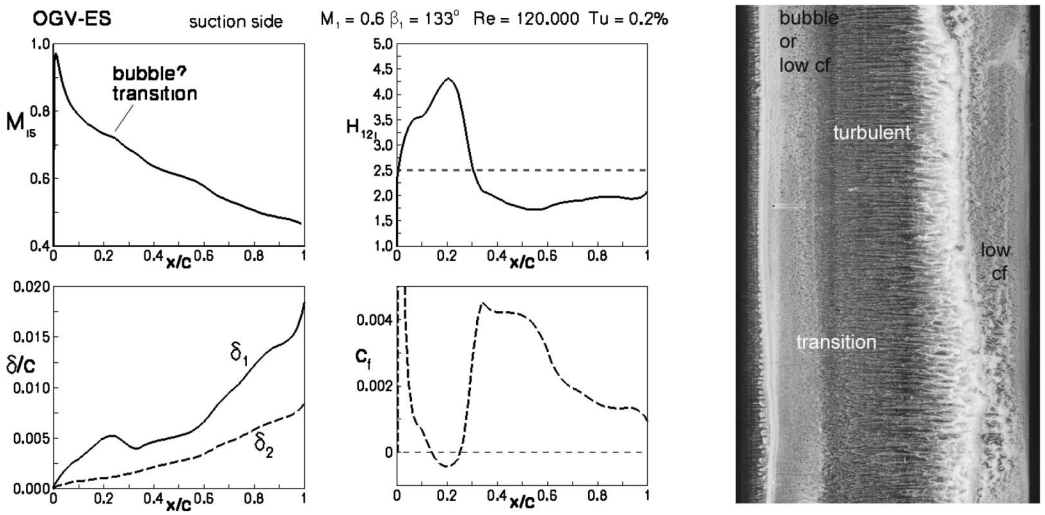

Fig. 17 MISES suction-side boundary layer parameters of OGV-ES blade and oil flow picture at $i=0$ deg and Re≈120,000

simulated form factors H_{12i} and the C_f distributions clearly reflect these two intermittently appearing situations, which seem to exist in parallel.

Oil streak lines and corresponding MISES boundary layer parameters for the two optimized blades are provided in **Figs. 17** and **18** for a Reynolds number around 120,000. The extremely front-loaded profile OGV-ES with its arbitrary leading edge starts with a flat laminar separation not immediately behind the LE but at approximately 6% of chord. From the oil picture it is difficult to decide whether there really is separation or just a transitional boundary layer with very low skin friction C_f. Downstream of about 22% the suction side is turbulent and there is no indication of a rear turbulent separation. The total pressure losses of this test achieve 3.8%. The corresponding MISES simulation required a turbulence level of 0.2% to approximate the low skin-friction region that is found on the front portion.

Behind the velocity peak of the MOGA blade, there is a short bubble (see the negative C_f values in **Fig. 18**), but the suction-side boundary layer remains laminar until it separates in a bubble at 31% and re-attaches at 53%. As the blade surface curvature underneath the bubble and the amount of adverse pressure gradient behind the separation point is relatively low, the bubble height and the resulting losses remain low too, [17]. However, toward the trailing edge the skin friction coefficient tends to zero, as a result of which the rear part of the oil is not moved ϑ. Overall total pressure losses at this low Reynolds number test are measured to be around 3.4%.

Conclusions

Two numerically optimized exit guide vane cascades designed for low Reynolds number conditions were tested and the results compared to a baseline cascade with controlled diffusion blades. Both the experimental and numerical results confirmed that the two different optimization methods were able to reduce the total pressure losses at design incidence and to increase the low loss incidence range in the positive direction by about 2–3 deg. Although the two optimized cascades show a considerably different geometry and loading distribution, losses at $\mathrm{Re}=1.0-1.2\times10^5$ could be reduced by about 60%. The superior performance in relation to the baseline CDA cascade was achieved because

a. the airfoils were designed with a more front-loaded pressure distribution and a reduced adverse pressure gradient along the suction side,

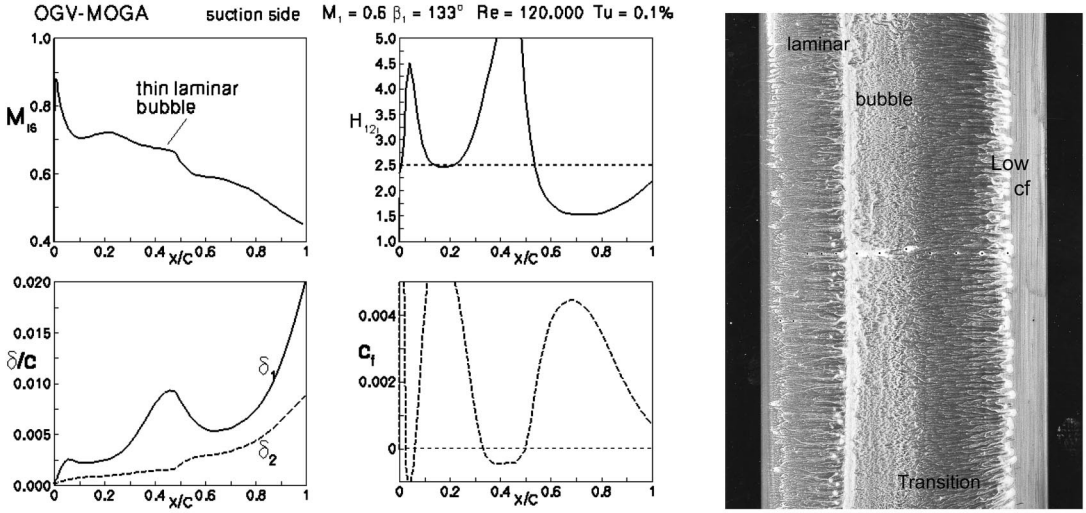

Fig. 18 MISES suction side boundary layer parameters of OGV-MOGA blade and oil flow picture at $i=0$ deg and Re≈120,000

b. the LE geometry was modified to avoid a concentrated LE peak with an intensive local separation,
c. in the region of a laminar separation bubble the surface curvature was reduced.

For blade chord Reynolds numbers well below 200,000 it seems to be advantageous to design the airfoils with a fairly steep adverse pressure gradient immediately at the front part in order to promote early transition to prevent the tendency for large laminar separations and the risk of bubble burst. The second obtained alternative, that has a slightly reduced front peak, still operates with laminar flow and a midchord separation bubble, but due to a reduced surface curvature underneath the bubble, its thickness and drag could be reduced considerably.

The Navier-Stokes solver embedded in the optimization process and employed for flow analysis allowed an excellent resolution of the low Reynolds number airfoil aerodynamics with LE bubble and midchord separation. Due to the implemented transition model, the low Reynolds number incidence characteristic was simulated reasonably well. At the same time, some improvements are still necessary to obtain better off-design characteristics especially at higher Reynolds numbers.

The authors are aware that in real turbomachinery environments the high turbulence level can alter the laminar separation behavior considerably, but some blade-to-blade calculations with a turbulence level of 5% revealed that even under the low Reynolds number conditions ($\mathrm{Re}=1.2\times10^5$) the present optimized blades both showed about 50% lower design point losses in relation to the baseline CDA blade.

This work demonstrated the intrinsic advantage of using automated blade optimizations even for complex low Reynolds number aerodynamics. The ability of the present design tools may still be limited, but they offer an essential advantage for the future. After further slight improvements, for example implementation of more problem oriented objective functions, these tools can be embedded in modern automated design processes for turbomachines and it will be possible to achieve new innovative configurations that could not be found by even very experienced design engineers.

Nomenclature

AVDR = axial velocity density ratio $=(\rho_2 w_2 \sin\beta_2)/(\rho_1 w_1 \sin\beta_1)$
D_f = diffusion factor $=1-w_2/w_1+(w_2/w_1{}^*\cos\beta_2\text{-}\cos\beta_1)s/2c$
c = chord length
C_f = friction coefficient $=2\tau_w/(\rho w^2)$
H_{12} = shape factor $=\delta_1/\delta_2$ (index i when incompressible)
i = incidence angle $=\beta_1-\beta_{1\,\mathrm{design}}$
M = Mach number
p = pressure
Re = Reynolds number based on chord length
s = blade spacing
w = velocity
x = chordwise coordinate
β = flow angle with respect to cascade front
δ_1 = boundary layer displacement thickness
δ_2 = boundary layer momentum thickness
ρ = density
ω = total pressure loss coefficient: $\omega=(p_{t1}-p_t)/(p_{t1}-p_1)$

Subscripts

1 = inlet plane, far upstream
2 = exit plane, far downstream
is = is isentropic entity
LE = leading edge
TE = trailing edge

References

[1] Rhoden, H. G., 1952, ''Effects of Reynolds Number on the Flow of Air Through a Cascade of Compressor Blades,'' ARC, R&M No. 2919.
[2] Roberts, W. B., 1975, ''The Effect of Reynolds Number and Laminar Separation on Axial Cascade Performance,'' ASME J. Eng. Gas Turbines Power, **97**, pp. 261–274.
[3] Roberts, W. B., 1979, ''Axial Compressor Blade Optimization in a Low Reynolds Number Regime,'' AIAA J., **17**(12), pp. 1361–1367.
[4] Selig, M. S., Gopalarathan, A., Giuere, P., and Lyon, C. A., 2001, ''Systematic Airfoil Design Studies at Low Reynolds Numbers,'' in *Fixed and Flapping Aerodynamics for Micro Air Vehicle Applications*, Prog. Astronaut. Aeronaut., **195**, pp. 143–167.
[5] Mueller, T. J., 1985, ''Low Reynolds Number Vehicles,'' AGARDograph No. 288, AGARD-AG-288.
[6] Sonoda, T., Yamaguchi, Y., Arima, T., Olhofer, M., Sendhoff, B., and Schreiber, H. A., 2003, ''Advanced High Turning Compressor Airfoils For Low Reynolds Number Condition, Part 1: Design and Optimization,'' ASME Paper GT-2003-38458.
[7] Olhofer, M., Arima, T., Sonoda, T., Fischer, M., and Sendhoff, B., 2001, ''Aerodynamic Shape Optimization Using Evolution Strategies,'' *Optimization in Industry III*, Springer-Verlag, New York.
[8] Yamaguchi, Y., and Arima, T., 2000, ''Multi-Objective Optimization for the Transonic Compressor Stator Blade,'' AIAA Paper 2000-4909.
[9] Arima, T., Sonoda, T., Shiratori, M., Tamura, A., and Kikuchi, K., 1999, ''A Numerical Investigation of Transonic Axial Compressor Rotor Flow Using a Low Reynolds number k-ε Turbulence Model,'' ASME J. Turbomach., **121**(1), pp. 44–58.
[10] Wilcox, D. C., 1988, ''Reassessment of the Scale-Determining Equation for Advanced Turbulence Models,'' AIAA J., **26**(11), pp. 1299–1310.
[11] Drela, M., and Youngren, H., 1991, ''Viscous/Inviscid Method for Preliminary Design of Transonic Cascades,'' AIAA Paper 91-2364.
[12] Drela, M., 1995, ''Implementation of Modified Abu-Ghannam Shaw Transition Criterion,'' *MISES User's Guide*, M.I.T., Computational Aerospace Science Lab., Cambridge, MA.
[13] Steinert, W., Eisenberg, B., and Starken, B., 1991, ''Design and Testing of a Controlled Diffusion Airfoil Cascade for Industrial Axial Flow Compressor Application,'' ASME J. Turbomach., **113**(4), pp. 583–590.
[14] Sanz, W., and Platzer, M. F., 1997, ''On the Calculation of Laminar Separation Bubbles Using Different Transition Models,'' ASME Paper 97-GT-453.
[15] Walraevens, R. E., and Cumpsty, N. A., 1995, ''Leading Edge Separation Bubbles on Turbomachine Blades,'' ASME J. Turbomach., **117**, pp. 115–125.
[16] Michelassi, V., Rodi, W., and Gieß, P.-A., 1998, ''Experimental and Numerical Investigation of Boundary-Layer and Wake Development in a Transonic Turbine Cascade,'' Aerosp. Sci. Technol., (**3**), pp. 191–204.
[17] Eppler, R., 1990, *Airfoil Design and Data*, Springer-Verlag, Berlin.